16 (2022) 100131

Contents lists available at ScienceDirect

Journal of Non-Crystalline Solids: X

journal homepage: www.sciencedirect.com/journal/journal-of-non-crystalline-solids-x

Microscopic structure and dynamics of glass forming Zr_2Co melts and the impact of different late transition metals on the melt properties

M.D. Ruiz-Martín [a,b], D. Holland-Moritz [a,*], F. Yang [a,*], C.C. Yuan [a,c], G.G. Simeoni [d], T.C. Hansen [b], U. Rütt [e,f], O. Gutowski [e], J. Bednarčík [e,g], A. Meyer [a,b]

[a] Institut für Materialphysik im Weltraum, Deutsches Zentrum für Luft- und Raumfahrt (DLR), 51170 Köln, Germany
[b] Institut Laue-Langevin (ILL), 38042 Grenoble, France
[c] School of Materials Science and Engineering, Jiangsu Key Laboratory for Advanced Metallic Materials, Southeast University, Nanjing 211189, China
[d] Forschungsneutronenquelle Heinz Maier-Leibnitz (FRM II), Technische Universität München, 85747 Garching, Germany
[e] DESY Photon Science, 22607 Hamburg, Germany
[f] Argonne National Laboratory, IL 60439, Lemont, USA
[g] Department of Condensed Matter Physics, Institute of Physics, P.J. Safarik University, Park Angelinum 9, 041 54, Kosice, Slovakia

ARTICLE INFO

Keywords:
Structure of liquids
Liquid metals and alloys
Self-diffusion in metals
Neutron diffraction and scattering
X-ray diffraction

ABSTRACT

We studied the short-range order and the atomic dynamics of stable and undercooled binary Zr_2Co alloy melts as well as their density and viscosity. The containerless processing technique of electrostatic levitation was used to achieve deep undercooling and to avoid contaminations. Static structure factors are determined by combining this technique with neutron and high energy X-ray diffraction. Co self-diffusion coefficients are measured by quasielastic neutron scattering. Our results reveal that the short-range order of the Zr_2Co melts closely resembles that previously observed for $Zr_{64}Ni_{36}$. We consider this as the origin of the very similar melt dynamics of these two alloys at same temperatures. On the other hand, the difference in the structure and dynamics when compared with those of Zr_2Cu and Zr_2Pd shows clearly that not only the atomic sizes, but also electronic properties or chemical bonding have an important influence on the melt properties of Zr-based glass forming melts.

PACS number(s): 61.20.−p, 61.25.Mv, 66.30.Fq, 61.05.F-, 61.05.cp

1. Introduction

Zr-based alloys have attracted broad interest because of their ability to form (bulk) metallic glasses even when cooling down the melts at moderate cooling rates. While the best glass-forming ability in metallic systems is found for some multi-component alloys, the less complex binary glass-forming systems are attractive for studies on the short-range order (SRO) and the atomic dynamics, aiming to find a microscopic understanding of the glass formation process.

In order to understand the processes that determine the macroscopic physical properties of the melt (such as density, viscosity, surface tension and electrical resistivity) or the solidification behavior on an atomic scale, a microscopic probe is necessary. Elastic neutron and X-ray diffraction are perfect tools to reveal properties like the chemical and the topological structure, and inelastic neutron scattering is well suited for studying dynamical properties like the self-diffusion coefficients. The first are obtained by measuring the (partial) structure factors, and the latter are accessible by analyzing the scattering law $S(Q,\omega)$ of quasielastic neutron scattering. SRO and atomic dynamics are of special importance for understanding the glass-formation from the liquid. Here, the nucleation of crystalline phases during cooling of a melt is avoided, such that the melt freezes under formation of an amorphous solid.

In the recent past there have been considerable efforts in studying the liquid short-range structure of some binary Zr-based alloy systems that are closely related with the more complex multi-component Zr-based systems forming bulk metallic glasses. While for part of these studies only total X-ray structure factors of limited explanatory power have been measured [1–3], there are other investigations in which at least some of the three partial structure factors were directly determined from the experiment in the liquid [4–7] and amorphous state [8]. These partial structure factors have served also as a starting point for numerical calculations on details of the structure-dynamics relation [9].

* Corresponding authors.
E-mail addresses: Dirk.Holland-Moritz@dlr.de (D. Holland-Moritz), fan.yang@dlr.de (F. Yang).

https://doi.org/10.1016/j.nocx.2022.100131
Received 30 August 2022; Received in revised form 31 October 2022; Accepted 15 November 2022
Available online 17 November 2022

When comparing the partial Bhatia-Thornton structure factors S_{NN} that describe the topological short-range order for Zr-rich melts of Zr-Cu and Zr-Ni at similar composition ($Zr_{64}Ni_{36}$ and Zr_2Cu) and temperature, marked differences are observed despite the fact that Ni and Cu are transition metals of similar atomic radii [5]. On the other hand, the S_{NN} recently determined for Zr_2Pd (ref. [6]) closely resembles that of Zr_2Cu (ref. [5]) although the Goldschmidt radius of Pd is about 8% larger than that of Cu, as displayed in Fig. 1. In order to account for the differences in the atomic radii of the early transition metals here we have plotted S_{NN} as a function of Q/Q_0, where Q_0 is the position of the main maximum of S_{NN}. The behavior shown in Fig. 1 clearly shows that aspects different from simple arguments of packing, like chemical or electronic effects, decisively influence the SRO of Zr-based glass-forming melts. Despite the structural differences between liquid $Zr_{64}Ni_{36}$ on the one side and Zr_2Cu and Zr_2Pd on the other side, all these binary Zr-rich glass-forming melts are characterized by large nearest neighbor coordination numbers of $Z_{NN} > 13.6$. This also holds for melts of binary glass-forming $Nb_{40.5}Ni_{59.5}$ alloys [10]. These nearest neighbor coordination numbers are significantly larger than coordination numbers reported for monoatomic metallic melts ($Z \approx 12$) [11]. Because a short-range order dominated by aggregates of icosahedral, fcc or hcp structure implies $Z_{NN} = 12$, the much higher Z_{NN} observed for glass-forming Zr-Ni, Zr-Cu, Zr-Pd and Nb-Ni melts indicate that the SRO of these liquids cannot be dominated by such aggregates. Hence, the large coordination numbers are in contradiction to speculations [2,3,12–14] on a decisive role of an icosahedral SRO for glass-formation in such melts.

For alloy elements exhibiting a sufficiently large incoherent scattering cross section, like Ni and Cu in the case of Zr-Ni and Zr-Cu melts, quasielastic neutron scattering provides their precise self-diffusion coefficients, which has been reported for different alloy compositions [4,15,16]. For the Zr-Ni melts high activation energies for the Ni self-diffusion coefficients are found, ranging from $E_a = 0.64$ eV for Zr-rich $Zr_{64}Ni_{36}$ melts to $E_a = 0.76$ eV for Ni-rich $Zr_{36}Ni_{64}$ melts [15]. These large activation energies indicate sluggish atomic dynamics in liquid Zr-Ni that certainly favors glass-formation. However, for Zr-Cu melts that are characterized by an even better glass-forming ability, lower activation energies for Cu self-diffusion are observed ranging from $E_a = 0.42$ eV for Zr-rich Zr_2Cu melts to $E_a = 0.63$ eV for Cu-rich $Zr_{35.5}Cu_{64.5}$ melts [16]. Also the absolute values of the self-diffusion coefficients at same or similar Zr-composition and temperature are larger for the Cu self-diffusion in Zr-Cu melts than for the Ni self-diffusion in Zr-Ni liquids [16]. This clearly shows that sluggish atomic mobility is only one factor among others that favors glass formation. The faster atomic dynamics in liquid Zr-Cu may find its structural explanation in the smaller number density of molten Zr-Cu as compared to that of liquid Zr-Ni [16].

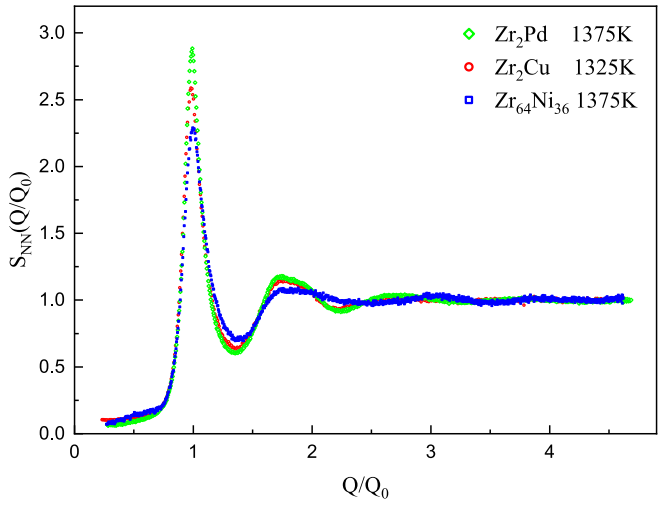

Fig. 1. Partial Bhatia-Thornton structure factor S_{NN} of Zr_2Pd [6], Zr_2Cu [5] and $Zr_{64}Ni_{36}$ [4] liquids as a function of Q/Q_0, where Q_0 is the position of the main maximum of S_{NN}.

In this paper besides a review of our previous works on the differences in the structure and/or dynamics of $Zr_{64}Ni_{36}$, Zr_2Cu, and Zr_2Pd melts, we present investigations on the structure and the atomic dynamics of binary melts of Zr with another transition metal, Co. Melts of the composition Zr_2Co are investigated by diffraction of neutron and synchrotron radiation in order to study the short-range order of the liquid phase as well as by quasielastic neutron scattering in order to examine the Co self-diffusion. This alloy composition corresponds to that of the congruently melting intermetallic phase Zr_2Co. For alloys whose self-diffusion cannot be studied by quasielastic neutron scattering, we present viscosity data in order to compare the dynamics of these melts. This addresses also the question how the microscopic scale properties and macroscopic structural and dynamical properties like the density or the viscosity of the liquids are related.

Of special importance with respect to glass-formation is the metastable regime of an undercooled melt at temperatures significantly below the melting temperature. In order to deeply undercool the melts heterogeneous nucleation at crucible walls or impurity sites must be suppressed. This can be achieved by containerless processing of the liquids under high vacuum conditions employing the electrostatic levitation (ESL) technique[17], which offers the additional advantages that reactions of the chemically highly reactive Zr-based melts with crucible materials are avoided and that background scattering at materials in the vicinity of the specimen is reduced in scattering experiments.

The role of chemical short-range order has been demonstrated in particular for Zr-Ni melts due to the full availability of the partial static structure factors of the liquid and its atomic dynamics. A theoretical link between the structure and dynamics has been established within the framework of mode coupling theory (MCT) for glass formation, using measured partial structure factors as an input [18]. The analysis shows that as a result of a strong chemical order in the melt the Zr and Ni diffusion proceeds with almost equal rates on the Zr-rich side. Hence it is more strongly coupled than one would expect for a binary hard-sphere mixture, where effects of chemical ordering are not included. When increasing the Ni concentration, a decoupling of the diffusion coefficients is observed [19]. The observed decoupling with increasing Ni-concentration can be explained by a saturation of the percentage of Zr-Ni neighbor pairs together with an increasing number of less strongly interacting Ni-Ni neighbors [7]. The mode coupling theory is also able to derive the observed temperature dependence of the self-diffusion coefficients in $Zr_{50}Ni_{50}$ from the temperature dependence of the measured partial structure factors [7]. Also, for the chemically similar $Ni_{65}Hf_{35}$ glass-forming alloy the difference in the melt dynamics can be understood based on an MCT analysis as a result of the small differences in the partial structure factors [9].

For Zr_2Co, Zr_2Cu, and Zr_2Pd melts, a complete set of partial structure factors has not been determined experimentally due to the lack of suitable isotopes for contrast variation in (elastic) neutron diffraction. Nevertheless, the SRO and the atomic dynamics characterize a liquid on a microscopic time- and length-scale. Hence, we discuss these structure-property relations based on the experimentally available results, including packing fraction derived from the melt density. With this, we cover the experimental possibilities to study the structure and dynamics of these glass forming alloys on both microscopic and macroscopic scales, and highlight that these differences cannot be explained simply by the (tabulated) atomic sizes.

2. Experimental details

Zr_2Co samples roughly 5 mm in diameter were prepared from the high purity constituents Co (99.998%) and Zr (99.97%) by arc melting under an argon 6 N atmosphere. For all scattering studies the samples were containerlessly processed under high vacuum conditions at total pressures smaller than $1 \bullet 10^{-6}$ mbar in an electrostatic levitation furnace

specially designed for neutron- or synchrotron scattering experiments. The high purity environmental conditions during levitation processing ensure that the samples are not contaminated from the environment even at long processing times of several hours. The temperature of the samples is contactlessly measured with an accuracy of ±5 K by use of a single-color pyrometer that is calibrated such that the liquidus temperature visible in the temperature-time profiles corresponds to the literature value of $T_L = 1323$ K. A detailed description of the ESL apparatus is given in ref. [20].

Elastic neutron scattering experiments on the SRO were performed on the high-intensity two-axis diffractometer D20 at the Institut Laue-Langevin (ILL) in Grenoble using a wavelength of the incident neutrons of $\lambda = 0.94$ Å. The static structure factors of the liquids, $S(Q)$, as function of the momentum transfer, Q, have been determined from the measured raw diffractograms by application of the same data evaluation procedure as described in ref. [21].

The X-ray diffraction studies were performed at beamline P7 of PETRA III at the German electron synchrotron (DESY) in Hamburg using monochromatic X-rays of 100 keV energy and a two-dimensional flat-panel detector (Perkin Elmer XRD 1621). The experimental setup is similar to that recently utilized for analogous experiments at beamline BW5 at DORIS III of DESY, which is described in ref. [5]. Calibrated and dark current corrected one dimensional intensity distributions, $I(Q)$, have been determined from the measured two dimensional intensity data by using the FIT2D [22,23] software package. From $I(Q)$ total structure factors, $S(Q)$, are calculated after subtraction of the background measured with the empty levitator, and correcting for self-absorption, Compton scattering, multiple scattering, polarization, and oblique incidence by utilizing the PDFget2X [24] analysis software.

For the investigation of the atomic dynamics of the liquids, quasielastic neutron scattering experiments were performed on the time of flight spectrometer TOFTOF [25] at the Research Neutron Source Heinz Meier-Leibnitz (FRM II) in Garching. The incident neutron wave length was set to 7.0 Å, combined with a chopper speed of 6000 rpm. This provided an energy resolution of 70 μeV. This energy resolution has been determined from the full width at half maximum (FWHM) obtained for the incoherent scattering of a solid Vanadium sphere with dimensions matching those of the sample subject of the study. It has been verified that the precise determination of diffusion coefficients is not hampered by influences of multiple scattering, even for strongly incoherent scattering samples like those of pure Ni with a large diameter of approx. 7.5 mm [26].

The temperature dependence of the density of liquid Zr_2Co was determined in an electrostatic levitation facility by employing a video imaging technique that is described in refs. [27] and [28]. The overall uncertainty in the numerical value of the obtained density is of about 1% (±0.5%), mainly limited by pixel size of the camera used. For determining the temperature dependence (thermal expansion), where only relative changes are compared, the precision is even higher. The viscosities of Zr_2Co and Zr_2Cu melts have been measured as a function of temperature by application of an oscillating droplet technique in the same electrostatic levitation device as described in ref. [28].

3. Results and discussion

3.1. The short-range order of liquid Zr-Co

The total structure factors of liquid Zr_2Co measured at different temperatures by neutron scattering, $S_N(Q)$, and X-ray diffraction, $S_X(Q)$, are plotted in Fig. 2. Because the synchrotron experiments require much shorter acquisition times (1 s) than the neutron scattering experiments (~30 min), a considerably broader temperature range could be covered by X-ray diffraction. Nevertheless, also by neutron scattering, measurements in the metastable regime of an undercooled melt could be performed at temperatures approximately 100 K below the liquidus temperature of $T_L = 1323$ K.

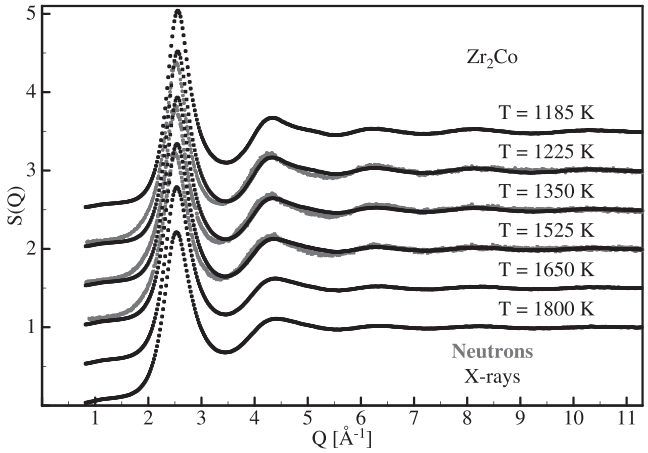

Fig. 2. Total structure factors $S_N(Q)$ measured by neutron scattering (gray) and $S_X(Q)$ measured by X-ray diffraction (black) for liquid Zr_2Co at different temperatures. The curves are shifted by multiples of 0.5 along the vertical axis.

S_N and S_X measured at same temperatures differ significantly with respect to the positions of the extrema of the curves (which occur at smaller Q for the neutron scattering measurements as for the X-ray diffraction measurements) as well as the shape of the second oscillation. This shows that the elements Zr and Co are not randomly distributed in the liquid, since the relative sensitivity to Co and Zr is different for X-rays and neutrons. When decreasing the temperature, T, the $S(Q)$ shows only gradual changes in a way that the characteristic features become more pronounced. This also indicates that no discontinuous changes of the SRO occur in the broad temperature ranges investigated by X-ray diffraction that includes temperatures above T_L and in the metastable regime of the undercooled liquid below T_L.

For melts of the alloy $Zr_{64}Ni_{36}$ the full set of partial structure factors has been determined by application of an isotopic substitution technique at a temperature of $T = 1375$ K [4]. The data of ref. [4] has been measured using an electromagnetic levitation facility. As discussed in ref. [20], the comparison with data measured in an electrostatic levitator indicates that for the electromagnetic levitation data there occurs some incoherent background scattering presumably due to secondary scattering at the water-cooled levitation coil. This incoherent contribution amounts to only about 10% of the intensity measured at large Q. The partial structure factors used for the following analysis result from a re-evaluation of the data of ref. [4], for which this effect is taken into account.

Using these partial structure factors of liquid $Zr_{64}Ni_{36}$ it is possible to construct the total neutron and X-ray structure factors of a hypothetic Zr_2TM melt that has the same partial Faber-Ziman structure factors as $Zr_{64}Ni_{36}$ but for which the late transition metal (TM) component has the same neutron scattering length and the same atomic X-ray scattering factor as Co. The total X-ray and neutron structure factors S'_X and S'_N of this hypothetical liquid are compared in Fig. 3a and b with S_X and S_N measured at a similar temperature of $T = 1350$ K for the real Zr_2Co melt. With the exception of a slightly smaller amplitude of the oscillations for S'_X and S'_N, the shape of the S_X and S_N is well reproduced. This indicates a similar short-range order in liquid Zr_2Co and $Zr_{64}Ni_{36}$. The same conclusions can be drawn if one assumes that the Co-Co partial structure factor $S_{Co\text{-}Co}$ is the same as $S_{Ni\text{-}Ni}$ in the $Zr_{64}Ni_{36}$ melt and then calculates the corresponding $S_{Zr\text{-}Zr}$ and $S_{Zr\text{-}Co}$ partial structure factors from the neutron and X-ray measurements. These partial structure factors closely resemble their counterparts in Zr-Ni, as shown in Fig. 3c and d. Consequently, the main conclusions on the short-range order drawn in ref. [4] from the partial structure factors of $Zr_{64}Ni_{36}$ apply also for Zr_2Co, including the finding that the short-range order of the melts is not dominated by icosahedral aggregates. In the light of the similar Goldschmidt radii of Ni and Co ($r_{at} \approx 1.25$ Å) [29] the structural similarity of

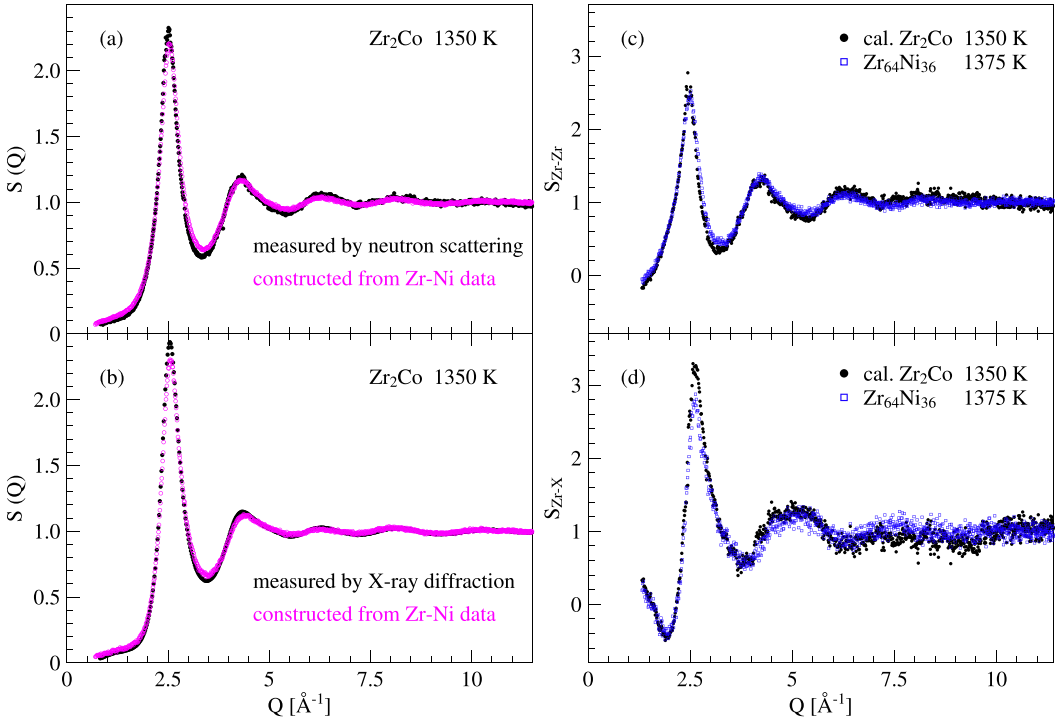

Fig. 3. Total structure factors measured by (a) neutron scattering and (b) X-ray diffraction for liquid Zr_2Co at $T = 1350$ K (black curves) and total structure factors constructed from the partial Faber-Ziman structure factors of $Zr_{64}Ni_{36}$ melts assuming that the late transition metal component scatters like Co (pink curves). (c) and (d) show a comparison of the partial structure factors S_{ZrZr} and S_{ZrX} (X = Ni,Co) in Zr_2Co and $Zr_{64}Ni_{36}$. For Zr_2Co these were calculated from the structure factors measured with neutrons and X-rays under the assumption that S_{CoCo} is the same as S_{NiNi} in $Zr_{64}Ni_{36}$. (For interpretation of the references to color in this figure legend, the reader is referred to the web version of this article.)

liquid Zr-Co and Zr-Ni is certainly not astonishing. Nevertheless, taking into consideration the pronounced structural differences found between melts of Zr_2Cu and $Zr_{64}Ni_{36}$ (ref. [5], also shown in Fig. 1), despite the fact that Cu, Ni, Co are neighbors in the periodic table and having similar atomic radii, it is evident that these short-range orders are not determined by atomic size only.

One parameter often discussed when dealing with the glass-forming ability of alloy melts is the enthalpy of mixing between the constituents of the melts [30]. One may wonder if there is a relation between this parameter and the structural differences between liquid Zr-Cu and Zr-Pd on the one side and liquid Zr-Ni and Zr-Co on the other side. In fact, the comparison of the values for the enthalpy of mixing of the different atomic pairs ($\Delta H^{mix}_{ZrNi} = -49$ kJ/mol, $\Delta H^{mix}_{ZrCo} = -41$ kJ/mol, $\Delta H^{mix}_{ZrCu} = -23$ kJ/mol $\Delta H^{mix}_{ZrPd} = -91$ kJ/mol) [30] may indicate that Ni and Co are chemically alike. Nevertheless, no clear correlation between enthalpy of mixing and the short-range order is found. For instance, Zr-Cu shows the lowest negative value of ΔH^{mix} among the four different melts, while Zr-Pd has the highest one, but both melts are characterized by the very similar topological short-range order.

In a recent work the short-range order and the electronic structure of Zr_2Co, Zr_2Ni, Zr_2Cu and Zr_2Ag melts have been studied by first-principles molecular dynamics simulations [31]. Partial pair correlation functions have been determined for the different melts. It is reported that the tendency of intermixing is highest for Zr_2Co, followed by Zr_2Ni, Zr_2Cu and finally Zr_2Ag and that the density of states of the *d* electrons of the late transition metal atoms shows the same sequence. We have calculated partial structure factors from the partial pair correlation functions of ref. 31 by Fourier transformation. From these we have calculated the corresponding total X-ray and neutron structure factors within the Faber-Ziman formalism using the corresponding neutron scattering lengths and x-ray scattering factors. As shown in Fig. 4 the simulated data for undercooled liquid Zr_2Co at $T = 1283$ K are able to reproduce our experimental findings at 1350 K or 1285 K reasonably well. Nevertheless, when going to high temperatures around $T = 1800$ K, the first principle molecular dynamics simulations predict more pronounced structural changes that are not consistent with the weak temperature dependence as shown in Fig. 4.

3.2. *Density of molten Zr_2Co*

The density is a macroscopic property of matter that is directly related with the atomic structure. In Fig. 5 the mass density measured for liquid Zr_2Co is plotted as a function of temperature. It shows a linear temperature dependence that is described by the equation $\rho(T) = ((-3.13 \pm 0.01)\bullet10^{-4} \bullet (T\text{-}T_L) + 6.82 \pm 0.03)$ g/cm^3, with a liquidus temperature of $T_L = 1323$ K. This corresponds to a temperature dependence of the number density given by $\rho_N(T) = ((-2.341 \pm 0.007)\bullet10^{-6} \bullet(T\text{-}T_L) + 0.0510 \pm 0.0002)$ at./Å^3. Huang et al [31] obtained in the first-principles molecular dynamics simulation 6.91 g/cm^3 at 1283 K and 6.79 g/cm^3 at 1830 K, which is quite close to our results, although the deviation towards high temperature is larger, shown in Fig. 5. This is in line with the observed larger deviation in the structure factors at 1830 K. At the same temperature, these values for the number density are only slightly lower than the number densities reported for melts of $Zr_{64}Ni_{36}$ ($\rho_N(T) = ((-2.825 \pm 0.008)\bullet10^{-6} \bullet(T\text{-}T_L) + 0.0521 \pm 0.0002)$ at./Å^3 (ref. [28], with $T_L = 1283$ K). The similar values for this macroscopic property of the liquids find a microscopic explanation in the resemblance of the short-range structures of the liquids as evidenced by the results of the diffraction experiments. On the other hand, at same temperatures the number densities reported for Zr_2Cu ($\rho_N(T) = ((-2.604 \pm 0.010)\bullet10^{-6} \bullet(T\text{-}T_L) + 0.0495 \pm 0.0001)$ at./Å^3 (ref. [16]), $T_L = 1286$ K) and Zr_2Pd: ($\rho_N(T) = ((-2.623 \pm 0.008)\bullet10^{-6} \bullet(T\text{-}T_L) + 0.0483 \pm 0.0002)$ at./Å^3 (ref. [6]), $T_L = 1358$ K) are smaller than those observed for Zr_2Co and $Zr_{64}Ni_{36}$ (see inset of Fig. 5).

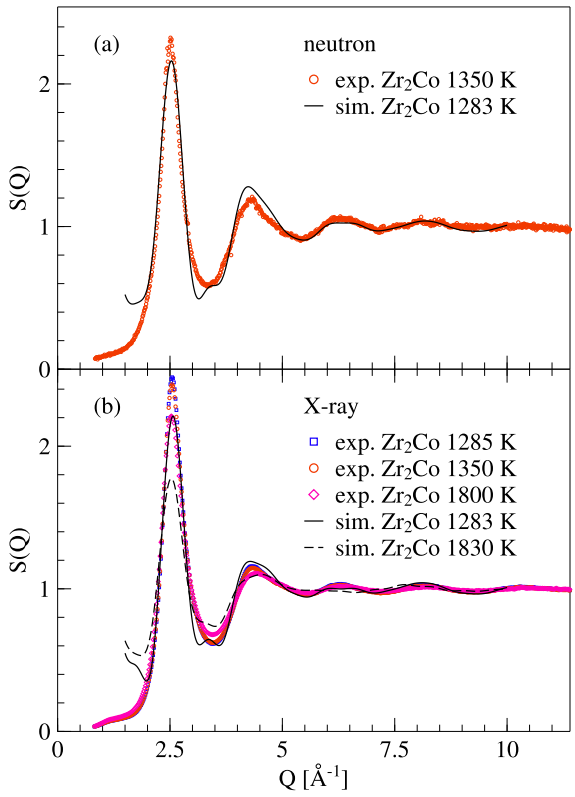

Fig. 4. Comparison between total structure factors for liquid Zr_2Co obtained by the first-principles molecular dynamics simulations of ref. [31] with those measured by neutron scattering (a) and by X-ray diffraction (b). The total structure factors of the simulation are calculated from the partial g(*r*)s using the corresponding neutron scattering lengths and and X-ray scattering factors. For the neutron total structure factors the comparison is performed at a slightly different temperature as no experimental result is available at 1283 K. However, as it can be seen from the X-ray total structure factors, the temperature dependence is quite weak.

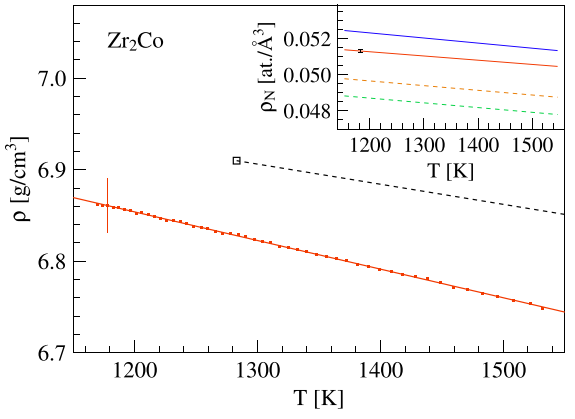

Fig. 5. Measured mass density of liquid Zr_2Co as a function of the temperature and a linear fit to the data points. The open square and the black dashed line show the density value and its temperature dependence obtained in the first-principles MD simulations of Huang et al. (ref. [31]). The inset shows the temperature dependence of the number density for liquid Zr_2Co (full red line), $Zr_{64}Ni_{36}$ (full blue line, ref. [28]) Zr_2Cu (dashed orange line, ref. [16]) and Zr_2Pd (dashed green line, ref. [6]). Error bars show the uncertainty of the numeric values of the density, valid for all the measured data points. (For interpretation of the references to color in this figure legend, the reader is referred to the web version of this article.)

3.3. The atomic dynamics of liquid Zr_2Co

Quasielastic neutron scattering measurements were performed for melts of Zr_2Co at different temperatures ranging from temperatures above the liquidus temperature ($T_L = 1323$ K) down to temperatures of $T = 1093$ K, in the metastable regime of the undercooled liquid. In Fig. 6 a set of quasielastic spectra is displayed. In the upper part of the figure the quasielastic spectra $S^*(Q,\omega)$ measured at fixed momentum transfer $Q = 0.6$ Å^{-1} at different temperatures are depicted, while in the bottom part of the figure the spectra measured at a fixed temperature ($T = 1343$ K) are shown for different wave vectors ranging from 0.3 Å^{-1} up to 1.3 Å^{-1}.

In all cases the quasielastic signal can be well described by

$$S^*(Q,\omega) = \frac{A}{\pi}\frac{\Gamma_{1/2}(Q)}{(\hbar\omega)^2 + \left(\Gamma_{1/2}(Q)\right)^2} \otimes \Re(Q,\omega) + b(Q)$$

which is a Lorentzian function of amplitude A convoluted with the instrumental energy resolution function $\Re(Q,\omega)$ measured at 290 K using a Vanadium standard (lines in Fig. 6). $b(Q)$ accounts for energy independent contributions to the signal and $\Gamma_{1/2}(Q)$ is the half width at half maximum (HWHM) of the Lorentzian curve, as described in ref [32]. $\Gamma_{1/2}$ of the Lorentzian function at constant Q increases with increasing temperature. If the temperature is constant, $\Gamma_{1/2}$ rises if Q is increased. Fig. 7 shows $\Gamma_{1/2}$ for different temperatures as a function of Q^2.

For small momentum transfer (below $Q \approx 1$ Å^{-1}) the measured signal is dominated by the incoherent scattering of the Co atoms (incoherent

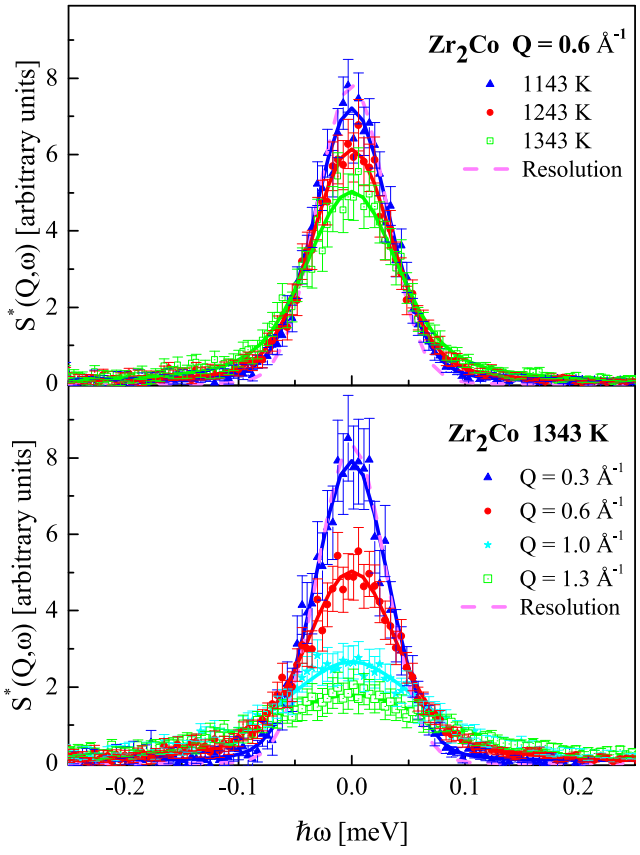

Fig. 6. (Color online) Quasielastic spectra for liquid Zr_2Co at $Q = 0.6$ Å^{-1} for different temperatures (upper part) and at $T = 1343$ K for four different wave vectors between $Q = 0.3$ Å^{-1} and $Q = 1.3$ Å^{-1} (lower part). The dashed line shows the instrument resolution function measured on the vanadium standard. The solid lines show the fits with a Lorentzian function convoluted with the instrumental energy resolution.

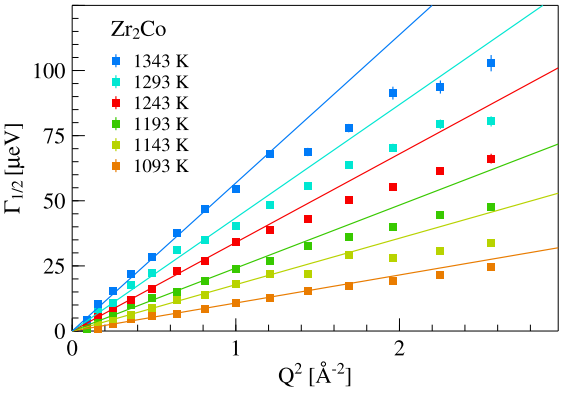

Fig. 7. (Color online) Half width at half maximum, $\Gamma_{1/2}$, of the Lorentzian curves as a function of Q^2 for liquid Zr_2Co at six different temperatures. The errors are smaller than the symbol size. The solid lines represent the linear fit characteristic of Fickian diffusion.

scattering cross sections: $\sigma_{inc}(Co) = 4.8$ b, $\sigma_{inc}(Zr) = 0.02$ b) and the mean Co self-diffusivity is related with $\Gamma_{1/2}$ by $D = \Gamma_{1/2}\, Q^{-2}/\hbar$ [33,34]. Hence, at small Q, the $\Gamma_{1/2}(Q^2)$ curves of Fig. 7 show a linear behavior and the slopes of the linear fits give the Co self-diffusivities. The deviations from the linear behavior at larger Q are due to coherent contributions to the scattered intensity that significantly increase when approaching the structure factor maximum. Therefore, for determining the Co self-diffusivities the linear fits are performed in the Q range between 0.3 and 1 $Å^{-1}$. The obtained values are compiled in Table 1 and plotted in Fig. 8 as a function of temperature. Also shown in Fig. 8 are results from former measurements of the Ni self-diffusivity in $Zr_{64}Ni_{36}$ (refs. [4,20]), of the Cu self-diffusivity in Zr_2Cu (ref. [16]), and of the mean Ni, Cu and Ti self-diffusivity in melts of glass-forming $Zr_{41.2}Ti_{13.8}Cu_{12.5}Ni_{10}Be_{22.5}$ (ref. [35]) and $Zr_{46.75}Ti_{8.25}Cu_{7.5}Ni_{10}Be_{27.5}$ (ref. [36]). Obviously, the values for the Co self-diffusivity in liquid Zr_2Co are almost identical with the values for the Ni self-diffusivity in $Zr_{64}Ni_{36}$ at same temperature. Similar as the curve for the Ni self-diffusivity in $Zr_{64}Ni_{36}$, the $D(T)$ curve for the Co self-diffusivity in Zr_2Co melts partly overlaps with the $D(T)$ curves determined for the mean Ti, Cu and Ni self-diffusivity in multi-component bulk metallic glass-forming $Zr_{41.2}Ti_{13.8}Cu_{12.5}Ni_{10}Be_{22.5}$ and $Zr_{46.75}Ti_{8.25}Cu_{7.5}Ni_{10}Be_{27.5}$ melts that are both well described by a $(T\text{-}T_c)^{\gamma}$ law with $T_c = 850$ K and $\gamma = 2.5$ (line in Fig. 8) [35]. In the investigated temperature range the diffusivity values determined for Zr_2Co are also well described by this curve.

Due to the fact that for the Zr-Co melts the full set of partial structure factors is not available, we cannot perform an analysis of the atomic dynamics in the framework of the mode coupling theory of the glass transition as performed for melts of Zr-Ni [7,18] or Hf-Ni [9]. Even though it was found that already slight variations of the partial structure factors may result in a significant change of the atomic dynamics [7], the structural resemblance of liquid Zr-Co and Zr-Ni observed by our diffraction studies may provide an explanation for the similar atomic

Table 1
Co self-diffusion coefficients of Zr_2Co melts determined by quasielastic neutron scattering at different temperatures below and above the liquidus temperature of $T_L = 1323$ K.

T [K]	D [10^{-9} m^2/s]
1093 ± 5	0.17 ± 0.02
1143 ± 5	0.27 ± 0.04
1193 ± 5	0.38 ± 0.04
1243 ± 5	0.53 ± 0.03
1293 ± 5	0.71 ± 0.05
1343 ± 5	0.94 ± 0.06

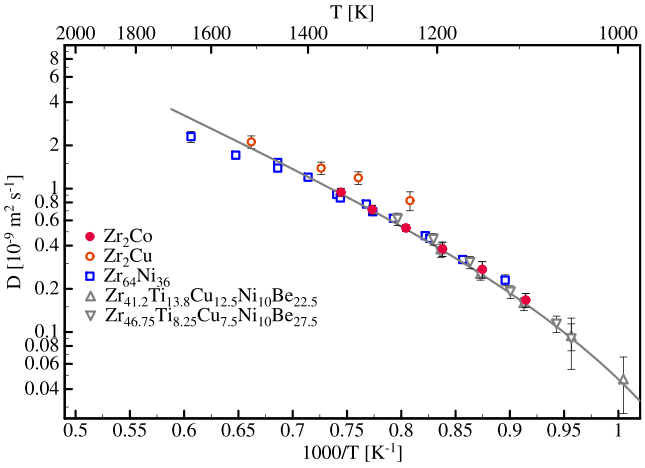

Fig. 8. Temperature dependence of the Co self-diffusivity in liquid Zr_2Co, of the Ni self-diffusivity in molten $Zr_{64}Ni_{36}$ (refs. [4,20]), of the Cu self-diffusivity in liquid Zr_2Cu (ref. [16]) and of the mean Ni, Cu and Ti self-diffusivities in liquid $Zr_{41.2}Ti_{13.8}Cu_{12.5}Ni_{10}Be_{22.5}$ (ref. [35]) and $Zr_{46.75}Ti_{8.25}Cu_{7.5}Ni_{10}Be_{27.5}$ (ref. [36]).

dynamics in both systems. On the other hand, the short-range order of Zr_2Cu differs significantly from that found in Zr_2Co and $Zr_{64}Ni_{36}$. As shown in Fig. 8 the Cu self-diffusivity in liquid Zr_2Cu is significantly larger than the Co and Ni self-diffusivity in Zr_2Co and, respectively, $Zr_{64}Ni_{36}$ at same temperature. This is in line with the lower number density of liquid Zr_2Cu as compared with Zr_2Ni and Zr_2Co (inset of Fig. 5), indicating the correlation between faster dynamics and lower packing. However, as will be shown later for the Zr_2Pd alloy, the effect of atomic size on the packing needs also be considered.

3.4. *Viscosity of Zr_2TM liquids*

The (shear) viscosity, η, of a liquid is a macroscopic property that is dependent on the atomic mobility. For those alloys whose incoherent neutron scattering cross sections are not sufficient to determine the self-diffusion coefficient by quasielastic neutron scattering, the viscosity provides a possibility to compare the dynamics of the different melts. In Fig. 9 the viscosity data measured for liquid Zr_2Co (ref. [39] are compared with results for melts of $Zr_{64}Ni_{36}$ (ref. [28], Zr_2Cu (this work), and Zr_2Pd (this work). Also shown in Fig. 9 are the best fits to the different sets of experimental data using the empirical Vogel-Fulcher-

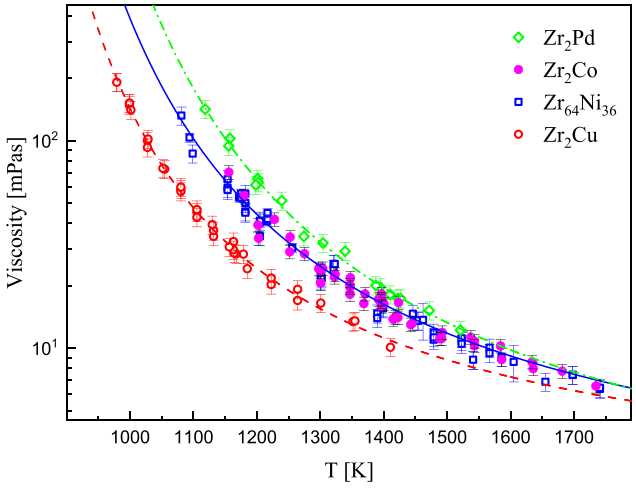

Fig. 9. Shear viscosity of liquid Zr_2Co (ref. [39]), $Zr_{64}Ni_{36}$ (ref. [28]), Zr_2Cu, and Zr_2Pd (both this work) as function of the temperature.

Tamman (VFT) law:

$$\eta(T) = \eta_0 exp\left(\frac{E_0}{k_B(T - T_0)}\right)$$

For molten Zr_2Co the best fit of the experimental data is obtained using the parameters $E_0 = (1.8 \pm 0.5)\bullet10^{-20}$ J, $T_0 = (783 \pm 76)$ K and $\eta_0 = (2.02 \pm 0.62)$ mPa s. For $Zr_{64}Ni_{36}$ (solid blue line) the parameters given in ref. [28] ($E_0 = (2.75 \pm 0.50)\bullet10^{-20}$ J, $T_0 = (660 \pm 47)$ K; $\eta_0 = (1.1 \pm 0.4)$ mPa s) are used. It should be noted that a discussion on the difference between the absolute values of the fitting parameters is not possible due to the comparatively large statistical errors of these parameters. Nevertheless, as shown in Fig. 9, the fitting-curve obtained from the viscosity data of $Zr_{64}Ni_{36}$ can well describe the data of liquid Zr_2Co in the investigated temperature range. Thus, here only the VFT-fitting for the $Zr_{64}Ni_{36}$ alloy is shown. Together with the finding that also the self-diffusion coefficients of Zr_2Co and $Zr_{64}Ni_{36}$ are on the same curve (Fig. 8), this indicates similar dynamic properties on microscopic and macroscopic length scale for both melts. This also immediately implies that for Zr_2Co the product $D\eta$ is a similar constant as for $Zr_{64}Ni_{36}$.

Compared to these two alloys, the viscosity of Zr_2Cu is lower, whereas the Zr_2Pd exhibits a higher melt viscosity. The corresponding VFT-fitting parameters are $E_0 = (1.93 \pm 0.16)\bullet10^{-20}$ J, $T_0 = (691 \pm 17)$ K and $\eta_0 = (1.58 \pm 0.22)$ mPa s for Zr_2Cu (red dashed line) and $E_0 = (3.30 \pm 0.94)\bullet10^{-20}$ J, $T_0 = (662 \pm 85)$ K and $\eta_0 = (0.76 \pm 0.45)$ mPa s for Zr_2Pd (green dash-dotted line). The faster macroscopic dynamics in Zr_2Cu suggested by the smaller viscosity are in good agreement with the larger self-diffusivities of the late transition metal component found for Zr_2Cu as compared to Zr_2Co and $Zr_{64}Ni_{36}$ that describe the dynamics on the atomic scale.

3.5. Structure-dynamics relations and glass forming ability

A densely packed melt is usually considered to favor glass formation, due to its more sluggish dynamics [37]. In order to compare between different liquids, a relatively simple, but only qualitative parameter, is the average packing fraction of the melt, φ:

$$\varphi = \rho_N \overline{V_a} = \rho_N \frac{4}{3}\pi \sum c_i r_i^3$$

with the number density ρ_N and the average atomic volume $\overline{V_a}$ calculated by assuming a certain atomic radius r_i of the i-th component and its corresponding concentration c_i. Using the covalent radii of these atoms [38], we derived a value of the packing fraction for Zr_2Cu of about 0.535 at 1200 K. It is lower than the packing fractions of Zr_2Co and $Zr_{64}Ni_{36}$ alloys both amounting to 0.547, whereas Zr_2Pd exhibits the highest packing fraction of 0.560. These observations are in line with the compositional trend of the melt viscosity, that a more densely packed melt exhibits more sluggish dynamics. However, the choice of covalent atomic radii is arbitrary for metallic melts, and it has been shown that such a correlation is not anymore observed when, for example, additional alloy elements like Al are involved [39].

From a microscopic point of view, in contrast to the similar structure and dynamics of the Zr_2Co and $Zr_{64}Ni_{36}$ melts, the underlying structural origin of the different melt viscosities between the Zr_2Cu and the Zr_2Pd liquids is not obvious based on the available structure data, considering that the S_{NN}, particularly their second oscillations, are rather similar as shown in Fig. 1. Here certainly a full set of partial structure factors is necessary in order to understand the liquid dynamics. This is similar to the Hf-Ni liquid when compared with the Zr-Ni alloys, where small differences in the liquid structure can result in different atomic dynamics [9].

The lowest liquid viscosity of Zr-Cu, the best glass forming system among the studied alloys, confirms again that the liquid dynamics are only one factor among others that determines the glass formation ability. Also, the significantly better glass-forming abilities of $Zr_{41.2}Ti_{13.8}Cu_{12.5}Ni_{10}Be_{22.5}$ and $Zr_{46.75}Ti_{8.25}Cu_{7.5}Ni_{10}Be_{27.5}$ do not correlate with the fact that they show similar dynamics as $Zr_{64}Ni_{36}$ and Zr_2Co. For the two multi-component alloys, at least one aspect to consider is that their liquidus temperatures are lower than those of the two binary ones. As a consequence, the atomic dynamics at the respective liquidus temperature is much slower.

4. Conclusions

We have determined the total structure factors of liquid Zr_2Co by diffraction of neutron and synchrotron radiation. The characteristic features of these total structure factors are well reproduced from the partial structure factors previously determined for $Zr_{64}Ni_{36}$ melts, when assuming an isomorphous substitution of Ni by Co. This indicates that liquid Zr_2Co is characterized by a similar short-range order as liquid $Zr_{64}Ni_{36}$. As a consequence of the similar short-range order also the average packing fraction, derived from the macroscopic density of the liquids, is similar at same temperature for both melts.

The atomic dynamics of stable and undercooled Zr_2Co melts were studied by quasielastic neutron scattering. The values of the Co self-diffusivity as function of temperature are on the same curve as the Ni self-diffusivity values reported for $Zr_{64}Ni_{36}$ melts and the mean Ti, Ni and Cu self-diffusivity values reported for glass-forming Zr-Ti-Ni-Cu-Be alloy melts. This may suggest that for these systems the self-diffusion of the incoherently scattering atoms is governed by similar microscopic processes. Furthermore, the shear viscosity values determined for liquid Zr_2Co as function of temperature are on the same curve as those of $Zr_{64}Ni_{36}$, indicating also a strong resemblance of these systems on the macroscopic time and length scale.

Taking into consideration that Co and Ni are neighbors in the periodic table of the elements and that both atoms are characterized by similar atomic radii, the close resemblance of the Zr-Ni and the Zr-Co melts, regarding the structural and dynamical properties, is in principle not astonishing. On the other hand, considering the mixing enthalpy, one may expect that Cu and Pd are chemically different when compared with Co and Ni. The observed structural and dynamical features of liquid Zr-Cu and Zr-Pd, which cannot be explained by simple arguments of packing, demonstrate that other effects, like electronic properties or chemical bonding, may have a decisive influence on the structural and dynamical properties in Zr-based melts. A full set of partial structure factors will be necessary to understand these differences, which requires further experimental as well as simulation/modelling efforts.

Declaration of Competing Interest

The authors declare that they have no known competing financial interests or personal relationships that could have appeared to influence the work reported in this paper.

Data availability

Data will be made available on request.

Acknowledgements

The authors thank J. Brillo, Z. Evenson, J. Gegner, P. Heintzmann, D. M. Herlach, I. Jonas, F. Kargl, and T. Voigtmann for fruitful discussions and/or support during the preparation and performance of the experiments, and E. Sondermann for a careful reading of the manuscript. The financial support provided by the Deutsche Forschungsgemeinschaft (DFG) under Grant No. ME1958/10-1 is gratefully acknowledged.

References

[1] A. Mizuno, T. Kaneko, S. Matsumura, M. Watanabe, S. Kohara, M. Takata, Mat. Sci. Forum 561–565 (2007) 1349.

[2] S.G. Hao, M.J. Kramer, C.Z. Wang, K.M. Ho, S. Nandi, A. Kreyssig, A.I. Goldman, V. Wessels, K.K. Sahu, K.F. Kelton, R.W. Hyers, S.M. Canepari, J.R. Rogers, Phys. Rev. B 79 (2009), 104206.
[3] V. Wessels, A.K. Gangopadhyay, K.K. Sahu, R.W. Hyers, S.M. Canepari, J.R. Rogers, M.J. Kramer, A.I. Goldman, D. Robinson, J.W. Lee, J.R. Morris, K.F. Kelton, Phys. Rev. B 83 (2011), 094116.
[4] D. Holland-Moritz, S. Stüber, H. Hartmann, T. Unruh, T. Hansen, A. Meyer, Phys. Rev. B 79 (2009), 064204.
[5] D. Holland-Moritz, F. Yang, T. Kordel, S. Klein, F. Kargl, J. Gegner, T. Hansen, J. Bednarcik, I. Kaban, O. Shuleshova, N. Mattern, A. Meyer, EPL 100 (2012) 56002.
[6] S. Klein, D. Holland-Moritz, D.M. Herlach, N.A. Mauro, K.F. Kelton, EPL 102 (2013) 36001.
[7] B. Nowak, D. Holland-Moritz, F. Yang, Th. Voigtmann, T. Kordel, T.C. Hansen, A. Meyer, Phys. Rev. Mater. 1 (2017), 025603.
[8] I. Kaban, P. Jóvári, V. Kokotin, O. Shuleshova, B. Beuneu, K. Saksl, N. Mattern, J. Eckert, A.L. Greer, Acta Mater. 61 (2013) 2509.
[9] B. Nowak, D. Holland-Moritz, F. Yang, Th. Voigtmann, Z. Evenson, T.C. Hansen, A. Meyer, Phys. Rev. B 96 (2017), 054201.
[10] D. Holland-Moritz, F. Yang, J. Gegner, T. Hansen, M.D. Ruiz-Martín, A. Meyer, J. Appl. Phys. 115 (2014), 203509.
[11] T. Schenk, D. Holland-Moritz, V. Simonet, R. Bellissent, D.M. Herlach, Phys. Rev. Lett. 89 (2002), 075507.
[12] H. Tanaka, J. Phys. Condens. Matter 15 (2003) L491.
[13] Y.Q. Cheng, H.W. Sheng, E. Ma, Phys. Rev. B 78 (2008), 014207.
[14] N. Jakse, A. Pasturel, Phys. Rev. B 78 (2008), 214204.
[15] D. Holland-Moritz, S. Stüber, H. Hartmann, T. Unruh, A. Meyer, J. Phys. Conf. Ser. 144 (2009), 012119.
[16] F. Yang, D. Holland-Moritz, J. Gegner, P. Heintzmann, F. Kargl, C.C. Yuan, G. G. Simeoni, A. Meyer, Europhys. Lett. 107 (2014) 46001.
[17] P.-F. Paradis, T. Ishikawa, G.-W. Lee, D. Holland-Moritz, J. Brillo, W.-K. Rhim, J. T. Okada, Mat. Sci. Eng. R 76 (2014) 1.
[18] T. Voigtmann, A. Meyer, D. Holland-Moritz, S. Stüber, T. Hansen, T. Unruh, Europhys. Lett. 82 (2008) 66001.
[19] S.W. Basuki, F. Yang, E. Gill, K. Rätzke, A. Meyer, F. Faupel, Phys. Rev. B 95 (2017), 024301.
[20] T. Kordel, D. Holland-Moritz, F. Yang, J. Peters, T. Unruh, T. Hansen, A. Meyer, Phys. Rev. B 83 (2011), 104205.
[21] D. Holland-Moritz, T. Schenk, P. Convert, T. Hansen, D.M. Herlach, Meas. Sci. Techn. 16 (2005) 372.
[22] A.P. Hammersley, ESRF Internal Report, ESRF98HA01T, FIT2D V9.129 Reference Manual V3.1, 1998.
[23] A.P. Hammersley, S.O. Swensson, M. Hanfland, A.N. Fitch, D. Häusermann, High Pressure Res. 14 (1996) 235.
[24] X. Qiu, J.W. Thompson, S.J.L. Billinge, J. Appl. Crystal. 37 (2004) 678.
[25] T. Unruh, J. Neuhaus, W. Petry, Nucl. Instr. Meth. A 580 (2007) 1414.
[26] A. Meyer, S. Stüber, D. Holland-Moritz, O. Heinen, T. Unruh, Phys. Rev. B 77 (2008), 092201.
[27] J. Brillo, I. Egry, Int. J. Thermophys. 24 (2003) 1155.
[28] J. Brillo, A.I. Pommrich, A. Meyer, Phys. Rev. Lett. 107 (2011), 165902.
[29] C.J. Smithells, in: E.A. Brandes (Ed.), Smithells Metals Reference Book, Butterworths, London, 1983.
[30] A. Takeuchi, A. Inoue, Mater. Trans JIM 41 (2000) 1372.
[31] L. Huang, C.Z. Wang, S.G. Hao, M.J. Kramer, K.M. Ho, Phys. Rev. B 81 (2010), 014108.
[32] A. Meyer, EPJ Web Conf. 83 (2015) 1002.
[33] J.P. Hansen, I.R. McDonald, Theory of Simple Liquids, Academic, London, 1976.
[34] J.P. Boon, S. Yip, Molecular Hydrodynamics, McGraw-Hill, New York, 1980.
[35] A. Meyer, W. Petry, M. Koza, M.-P. Macht, Appl. Phys. Lett. 83 (2003) 3894.
[36] F. Yang, T. Unruh, A. Meyer, Europhys. Lett. 107 (2014) 26001.
[37] A. Takeuchi, A. Inoue, Mater. Trans. 46 (2005) 2817.
[38] L. Pauling, J. Am. Chem. Soc. 69 (1947) 542.
[39] C.C. Yuan, F. Yang, F. Kargl, D. Holland-Moritz, G.G. Simeoni, A. Meyer, Phys. Rev. B 91 (2015), 214203.